Pyrazolium- *versus* imidazolium-based ionic liquids: structure, dynamics and physico-chemical properties

Cinzia Chiappe[*1] *Angelo Sanzone*,[1] *Daniele Mendola*,[2] *Franca Castiglione*,[2] *Antonino Famulari*,[2] *Guido Raos*,[2] *and Andrea Mele*[*2,3]

[1] Dipartimento di Chimica e Chimica Industriale - Università di Pisa, Via del Risorgimento, 35-56126 Pisa, Italy. E-mail: cinziac@farm.unipi.it [2] Department of Chemistry, Materials and Chemical Engineering "G. Natta", Politecnico di Milano, Piazza L. Da Vinci 32, 20132 Milano, Italy. [3] CNR – Istituto di Chimica per il Riconoscimento Molecolare, Via L. Mancinelli, 7, 20131 Milano; E-mail:andrea.mele@polimi.it

RECEIVED DATE (to be automatically inserted after your manuscript is accepted if required according to the journal that you are submitting your paper to)

* Author to whom correspondence should be addressed. E-mail: cinziac@farm.unipi.it. Ph.: +39-050-2219669. Fax: +39-050-2219660. E-mail: andrea.mele@polimi.it. Ph.: +39-02-23993006. Fax: +39-02-23993180.

ABSTRACT. Ionic liquids (ILs) composed of two different pyrazolium cations with dicyanamide and bis(trifluoromethanesulfonyl)imide anions have been synthesized and characterized by NMR, Kamlet-Taft solvatochromic parameters, conductivity and rheological measurements, as well as *ab initio* calculations. Density functional calculations for the two pyrazolium cations, 1-

butyl-2-methylpyrazolium [bmpz] and 1-butyl-2,3,5-trimethylpyrazolium [bm_3pz] provide a full picture of their conformational states. Homo- and heteronuclear NOE show aggregation motives sensitive to steric hindrance and anions' nature. Self-diffusion coefficients *D* for the anion and the cation have been measured by pulsed field gradient spin-echo NMR (PGSE-NMR). The ionic diffusivity is influenced by their chemical structure and steric hindrance giving the order $D_{cation} > D_{anion}$ for all the examined compounds. The measured ion diffusion coefficients, viscosities and ionic conductivity follow the Vogel-Fulcher-Tammann (VFT) equation for the temperature dependencies and the best fit parameters have been determined. Solvatochromic parameters indicate an increased ion association on going from bis(trifluoromethanesulfonyl)imide to dicyanamide-based pyrazolium salts, as well as specific hydrogen bond donor capability of H atoms on the pyrazolium ring. All these physical properties are compared to those of an analogous series of imidazolium-based ILs.

Keywords: pyrazolium, ionic liquids, solvatochromic parameters, NOE, diffusion, DFT calculations.

1. Introduction

Over the past ten years, room temperature ionic liquids (ILs) have aroused overwhelming interest due to their unique physico-chemical properties which make them useful in a broad range of applications: synthesis, (bio)catalysis, separation processes, electrochemistry, materials science, biotechnology and for the development of new electrical and electrochemical devices.[1] Generally composed by a bulky organic cation and a polyatomic anion, ILs are characterized by an extreme flexibility and modularity: it is possible to tailor their properties for specific applications through a suitable choice of the component ions. In recent years, new ILs have been

designed and synthesized to achieve important targets such as obtaining liquid salts characterized by low viscosity, high conductivity, high electrochemical stability associated with low flammability and low volatility. Despite of the wide selection of cations and anions giving ILs, those based on 1,3-dialkylimidazolium cations have dominated the field, probably due to their wide liquid range, high conductivities and low viscosities which are necessary for a multitude of applications.[2] The remarkable number of studies carried out on these salts have shown that their properties can be finely modulated by varying the alkyl groups, introducing specific groups on the cation or changing the nature of the anion. Moreover, experimental measurements and theoretical calculations have demonstrated that, depending on anion structure, imidazolium-based ILs can give highly structured ion networks,[3] in which polar and non-polar domains can be formed as a function of the cation's alkyl chain lengths.[4] A high degree of structural and dynamic heterogeneity has been evidenced both in the bulk and at the interfaces of these ILs: the highly cohesive charged groups tend to segregate from the side chains if these are sufficiently long, resulting in liquids with a heterogeneous structure at the nanometer scale, offering both ionic and non-polar nano-scale environments. Experiments carried out on other classes of ILs show that the degree of self-organization characterizing these media depends however also on the cation and, for example, it decreases on going from imidazolium to pyrrolidinium salts.[5]

Pyrazolium-based ILs have been only marginally investigated[6-7] although these salts, structurally analogous to imidazolium based-ILs, are generally characterized by a relatively low viscosity and a high conductivity, associated with relevant electrochemical properties. From the structural viewpoint, the different position of the nitrogen atoms in the heteroaromatic ring compared to the imidazolium series is expected to influence the charge distribution and consequently the nanostructuration (if any) of pyrazolium based ILs[8], thus making these systems

appealing in our search for new modes of local ordering. This may prove to be useful for their applications as reaction media or as electrolytes in electrochemical devices.

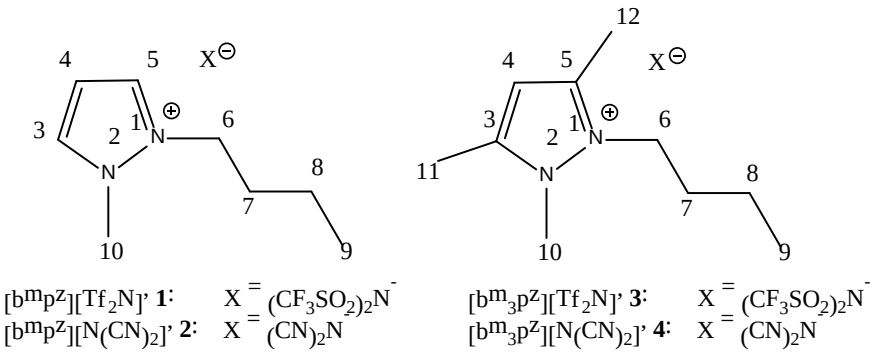

[$b^{m}p^{z}$][Tf_2N], **1**: X = $(CF_3SO_2)_2N^-$
[$b^{m}p^{z}$][$N(CN)_2$], **2**: X = $(CN)_2N$
[$b^{m}{}_{3}p^{z}$][Tf_2N], **3**: X = $(CF_3SO_2)_2N^-$
[$b^{m}{}_{3}p^{z}$][$N(CN)_2$], **4**: X = $(CN)_2N$

Scheme 1. Pyrazolium based-ILs

We have synthesized four different alkyl-substituted pyrazolium-based ILs: 1-butyl-2-methylpyrazolium bis(trifluoromethanesulfonyl)imide ([bmpz][Tf_2N], **1**), 1-butyl-2-methylpyrazolium dicyanamide ([bmpz][$N(CN)_2$], **2**), 1-butyl-2,3,5-trimethylpyrazolium bis(trifluoromethanesulfonyl)imide ([bm_3pz][Tf_2N], **3**) and 1-butyl-2,3,5-trimethylpyrazolium dicyanamide ([bm_3pz][$N(CN)_2$], **4**). Structures and atom numbers are shown in Scheme 1. We report the physicochemical characterization of these new systems and the comparison with the properties of analogous imidazolium salts. The structural and physicochemical properties are explored using modern two-dimensional NMR techniques and quantum chemical *ab initio* calculations. The main focus of the paper is the explanation of the ion transport properties, linking the observed cation/anion structure and interactions to the measured ionic diffusivity, viscosity and conductivity.

2. Experimental Section

2.1 IL Synthesis. The pyrazolium salts[1-4] were synthesized by methylation of pyrazole and 3,5-dimethylpyrazole with dimethylcarbonate in the presence of sodium methoxide at the reflux temperature, followed by alkylation of the resulting *N*-methyl derivatives with butyliodide, as shown in Scheme 2. Anion exchange on 1-butyl-3-methylpyrazolium iodide and 1-butyl-2,3,5-trimethylpyrazoliumiodide was carried out in water using $LiTf_2N$ or freshly prepared $Ag[N(CN)_2]$, according to literature procedures. The synthesized salts were characterized by ^1H NMR, ^{13}C NMR and ESI-MS.

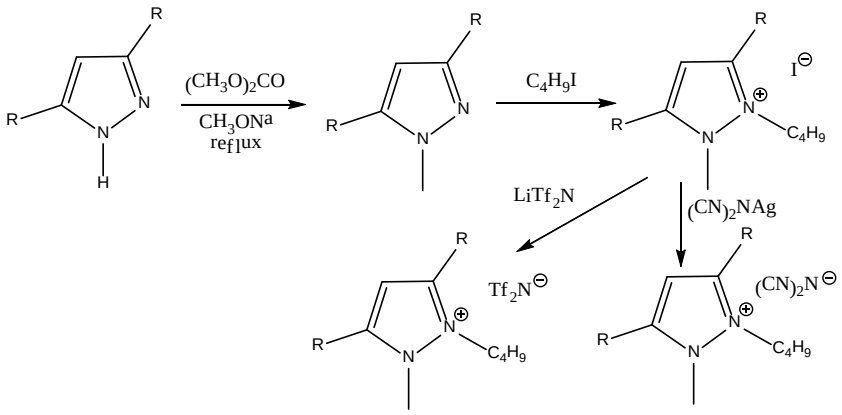

Scheme 2. Synthesis of the ILs.

2.2 NMR Measurements. All ionic liquids were dried for 5 h at 70 °C under mechanic pump vacuum before NMR experiments. NMR spectra were carried on a Bruker Avance 500 spectrometer operating at 500 MHz proton frequency and equipped with a QNP four nuclei switchable probe. Suitable amounts (0.5-1.0 g each) of dry **1**, **2** and **3** were transferred in a 5 mm NMR tube. A sealed capillary containing DMSO-d_6 was used as internal chemical shift reference. The NMR tubes were flame-sealed immediately after the transfer of ionic liquids. {^1H-^{19}F}HOESY experiments[9-10] were acquired using the inverse detected pulse sequence with 512 increments in the t1 dimension with 16 scans for each experiment, with a mixing time of 40 ms.

Two-dimensional correlation experiments by dipolar coupling in the rotating frame (ROESY) were performed using a pulse sequence with 700 increments in the t1 dimension with 16 scans for each experiment and a mixing time of 200 ms.

Self-diffusion coefficients were measured by pulsed field gradient spin-echo NMR (PGSE-NMR) experiments. A pulsed gradient unit capable of producing magnetic field pulse gradients in the z-direction of 53 G cm^{-1} was used. All the experiments were performed using the double stimulated echo pulse sequence[11] to suppress convection artifacts. The duration of the magnetic field pulse gradients (δ) and the diffusion times (Δ) were optimized for each sample in order to obtain complete dephasing of the signals with the maximum gradient strength. In each experiment, a series of 32 spectra with 16K points were collected. For the investigated samples, δ values were in the 2 ms and 6 ms ranges, respectively for ^{1}H and ^{19}F experiments, while the Δ values were in the 0,4 s and 0,8 s ranges, respectively for ^{1}H and ^{19}F experiments. The pulse gradients were incremented from 2 to 95% of the maximum gradient strength in a linear ramp. Temperature was controlled with an air flow of 535 L h^{-1} in order to avoid any temperature fluctuations due to sample heating during the magnetic field pulse gradients. Variable temperature experiments were performed changing the temperature from 300 K to 340 K in steps of 5 K.

***2.3 Conductivity, Viscosity and UV-VIS Measurements*.** Conductance measurements were performed using a CON 510 bench meter supplied with conductivity/TDS electrode equipped with a temperature sensor for automatic temperature compensation (cell constant of K = 1.0). Viscosity was measured for all the dicyanamide samples using Brookfield DV-II + Pro instrument. ESI-MS analyses were performed on a Finnigan LCQ Advantage (Thermo Finnigan, San Jose, CA, USA) ion trap instrument equipped with an Excalibur software.

Solvatochromic dyes like Reichardt's betaine dye, N,N-diethyl-4-nitroaniline and 4-nitroaniline were dissolved in ionic liquids. These were taken in a quartz cell with light path length of 1 mm on a Cary 2200 spectrophotometer (300-800 nm). Individual stock solutions of Reichardt's betaine dye, N,N-diethyl-4-nitroaniline and 4-nitroaniline were prepared in dichloromethane. In order to prepare a given dye/ionic liquid solution, the appropriate amount of the dye stock solution was micropipetted into a clean dry quartz cuvette. Residual dichloromethane was accurately evaporated under gentle stream of argon gas. The CH_2Cl_2 removal was checked by NMR by monitoring the peak at 5.3 ppm. The ionic liquid was then added to the cuvette. The cuvette was then capped and sealed and the sample was mixed for an appropriate time before the experimental measurements.

2.4 Computational Procedures. All calculations were performed with the GAMESS-US program.[12] Stable conformations of the cations were obtained by density functional theory (DFT)[13]. In particular, the B3LYP hybrid functional[14] and the standard 6-311G** basis set[15] were adopted. Three dihedral angles were defined in order to explore the conformational space of the butyl chain: α_1 (C(7)-C(6)-N(1)-C(5)), α_2 (C(8)-C(7)-C(6)-N(1)) and α_3 (C(9)-C(8)-C(7)-C(6)), as shown in Figure 1. For all the dihedrals, the *anti* (α = 180°), *gauche*+ (α = +60°) and *gauche*– (α = –60°) conformations were used as starting geometry and then fully minimized. Accordingly, 27 conformations for cations **1** and **3** were generated. The conformers are unambiguously identified by the triplet of α_1, α_2 and α_3 values. The angles, energies and populations of all conformations are given in Tables S1 and S2 of the Supplementary Information (SI).

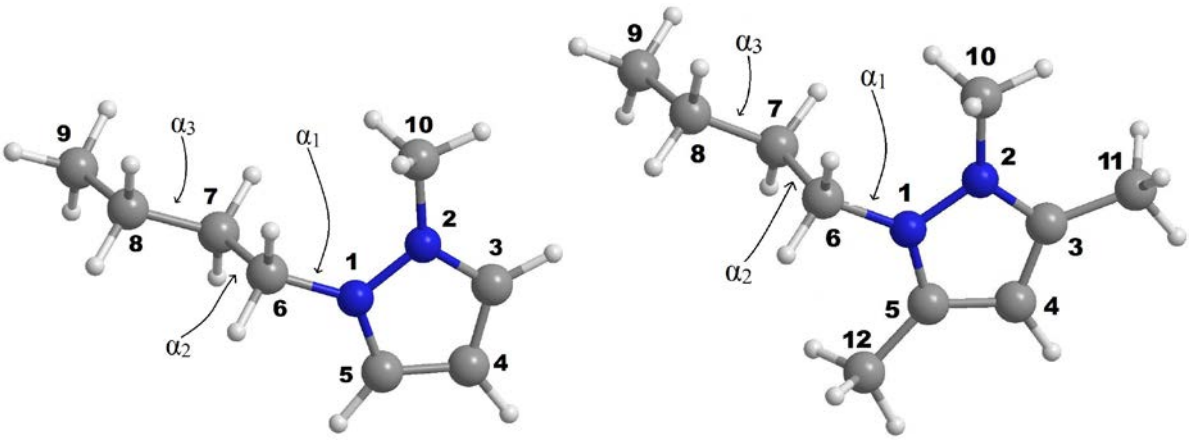

Figure 1. Definition of the dihedral angles α_1, α_2 and α_3 for the butyl chain of the examined compounds. The pictures show their optimized minimum-energy conformations.

Average interatomic distances, in which each conformation is weighted according to its Boltzmann population (see below), were calculated in order to support the interpretation of NOE data.[16] Details are given in the SI.

3. Results and Discussion

3.1 DFT Calculations. The main purpose of the DFT calculations is to provide average interatomic distances, suitable for the discrimination between inter- and intramolecular NOE data.[10] Nevertheless, the calculated structures deserve some comments considering that, at the moment, no literature data are available on pyrazole-based systems, including single crystal X-ray structures. At this stage of preliminary investigation on pyrazole-based ILs, it is interesting to compare them with the related and extensively studied 1-butyl-3methylimidazolium-based (bmim) analogues.

The DFT calculation on cations **1** and **3** show well-defined conformational properties of their butyl chain. The populations of the different conformers may be calculated according to Eq. (1):

$$P(\alpha_1,\alpha_2,\alpha_3) = \frac{e^{-E(\alpha_1,\alpha_2,\alpha_3)/kT}}{\sum_{\alpha_1}\sum_{\alpha_2}\sum_{\alpha_3} e^{-E(\alpha_1,\alpha_2,\alpha_3)/kT}} \quad (1)$$

where *k* is Boltzmann's constant, *T* is the absolute temperature (=298 K) and $E(\alpha_1,\alpha_2,\alpha_3)$ is total energy of a specific conformation. From the Boltzmann probabilities, the distribution for a single torsion angle (α_1, for example) were calculated as:

$$P(\alpha_1) = \sum_{\alpha_2}\sum_{\alpha_3} P(\alpha_1,\alpha_2,\alpha_3) \quad (2)$$

These distributions are displayed in the forms of histograms in Figure 2. For both pyrazole-based cations **1** and **3,** α_1 angle is centred around ±90°, arbitrarily labelled as up (u) or down (d). The corresponding conformers account for about the 80% of the population in **1**, 100% in **3**, where the in-plane arrangement of the side chain is forbidden by steric the hindrance of the methyl groups on either sides of N(1). These findings confirm that also in the pyrazolium cations the butyl chain preferentially assumes the out-of-plane conformation, similarly to what already found for the bmim derivatives, both by molecular dynamics (MD) simulations and NMR spectroscopy[17] and by solid state structural studies.[18-22]

Three major families of conformations in cations **1** and **3** can be identified on the basis of the distributions of α_2 and α_3: *anti-anti* (*tt*), *gauche-anti* (*gt*) and *anti-gauche* (*tg*). In grouping the conformers together, all the possible combinations of *gauche*+ and *gauche*– have been considered and summed up. For both pyrazole cations **1** and **3,** the families of conformations mentioned above account for about 82% of the overall population. The *tt* conformers are the most abundant class of rotamers for **1** (38.1%), whilst the *tg* conformers account for the 36.1% of the population of **3**. It is interesting to note that the calculations predict that also the *gauche*± conformations for α_3 are appreciably populated. The same was found for the butyl chain of bmim by MD and experimentally confirmed by NMR.[17] The conformational flexibility of the chain is

drastically reduced in the crystal state, where the α_3 dihedral of the butyl chain of a set of bmim derivatives was found to populate the *t* conformation only.[18-22] Examples of significantly populated conformations for **1** and **3** are showed in Figure S4 and S5 of SI, respectively.

At this preliminary stage of investigation on pyrazole-based ILs, DFT calculations indicate that the conformational properties of the butyl chain of cation of compounds **1** and **3** are similar to those of the homologous chain in the reference imidazolium cation. A good match is observed, despite of the fact that the comparison of DFT calculations on gas phase cations (this work) with MD data on bulk ionic liquid[17] is naturally biased by the different starting systems, the presence of the counterion, intermolecular interactions (in the case of [bmim][BF_4]), and computational approaches.

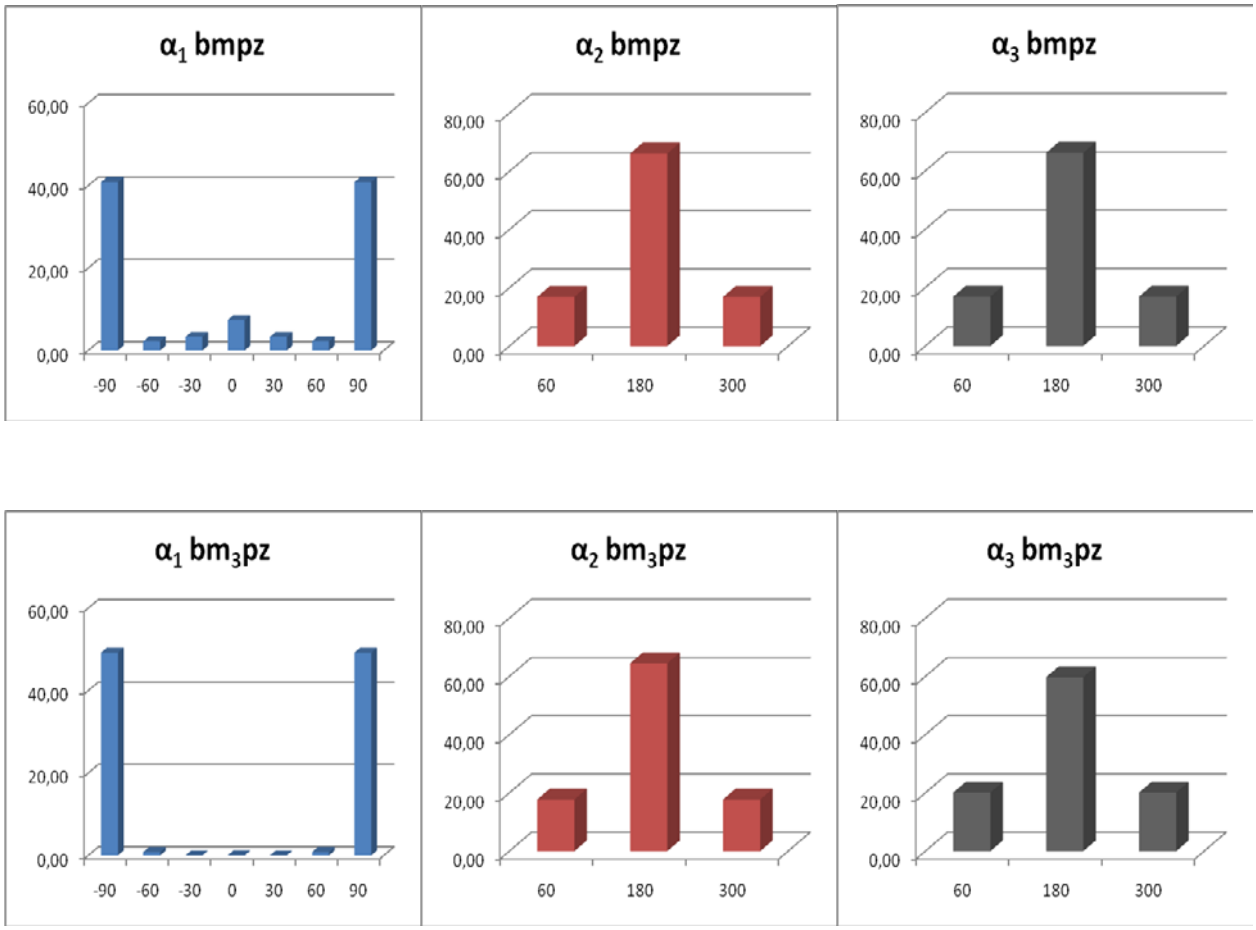

Figure 2. Histograms showing the distribution of the dihedral angles α_1, α_2 and α_3 calculated at DFT level for cation **1** (bmpz, top) and cation **3** (bm_3pz, bottom).

3.2 Internuclear Contacts via Nuclear Overhauser Enhancements. The main purpose of the NMR investigation is the assessment of possible aggregation motives in the bulk liquid, due to the presence of local order or nanostructuration.[4a] This can be done exploiting the intermolecular Nuclear Overhauser Effect (NOE). According to the methodological approach proposed by Oysteryoung and coworkers,[10] rotating frame NOE correlation experiments (ROESY) were carried out to observe specific cation-cation organization. This approach has been successfully applied several times in the study of the imidazolium series of ILs.[23-27] The separation of the intra- and intermolecular dipolar contacts can be done *a posteriori* by applying the distance threshold of 4 Å for vanishing ROEs. The average distances between the H atoms of interest in cations **1** and **3** were calculated at DFT level (see the SI) and used to assign intra- and intermolecular ROEs, *e.g.* detectable ROEs between protons more that 4 Å apart within the same cation should be considered as intermolecular contacts.

The intermolecular ROEs observed in the pure liquids **1**, **3** and **4** are summarized in Tables 1, 2 and 3, respectively.

Table 1. ROESY (^{1}H-^{1}H) intermolecular interactions for compound **1**. Legend: w = weak, m = medium, s = strong, * = no intermolecular interaction. Head-to-head and head-to-tail motives are indicated in the table with grey and striped cells, respectively.

	H3	**H4**	**H5**	**H6**	**H7**	**H8**	**H9**	**H10**
H3	**-**	*****	*****	**w**	*****	*****	**w**	*****

H4	*	-	*	*	*	*	w	m/s
H5	*	*	-	*	*	w	w	s
H6	w	*	*	-	*	*	w	*
H7	*	*	*	*	-	*	*	*
H8	*	*	w	*	*	-	*	w
H9	w	w	w	w	*	*	-	s
H10	*	m/s	s	*	*	w	s	-

Table 2. ROESY (^{1}H-^{1}H) intermolecular interactions for **3**; w = weak, m = medium, s = strong, * = no intermolecular interaction. Head-to-head and head-to-tail motives are indicated in the table with grey and striped cells, respectively.

	H11	H4	H12	H6	H7	H8	H9	H10
H11	-	*	*	*	*	*	m/w	*
H4	*	-	*	w	*	*	w	w
H12	*	*	-	*	*	w	*	*
H6	*	w	*	-	*	*	*	*
H7	*	*	*	*	-	*	*	*
H8	*	*	w	*	*	-	*	m
H9	m/w	w	*	*	*	*	-	w
H10	*	w	*	*	*	m	w	-

Table 3. ROESY (^{1}H-^{1}H) intermolecular interactions for **4**; w = weak, m = medium, s = strong, * = no intermolecular interaction. Head-to-head and head-to-tail motives are indicated in the table with grey and striped cells, respectively.

	H11	**H4**	**H12**	**H6**	**H7**	**H8**	**H9**	**H10**
H11	-	*	*	*	*	*	w	*
H4	*	-	*	w	*	*	w	m
H12	*	*	-	*	*	*	*	*
H6	*	w	*	-	*	*	*	*
H7	*	*	*	*	-	*	*	*
H8	*	*	*	*	*	-	*	*
H9	w	w	*	*	*	*	-	w
H10	*	m	*	*	*	*	w	-

The cations can be depicted as a polar head (the charged pyrazolium ring: C(3), C(4), C(5), C(6), C(10), C(11)) and an apolar tail (the *n*-butyl chain). Two distinct aggregation motives can be identified within the ROE matrices: head-to-tail (*h*-*t*) and head-to-head (*h*-*h*). The corresponding contacts are highlighted in the tables in different ways (grey for *h*-*h* interaction and striped for *h*-*t*), while those contacts which are likely to originate from both intra- and inter-molecular interactions are not considered.

Both *h*-*h* and *h*-*t* arrangements are present in all compounds. It is not straightforward to assign a relative weight to these arrangements on the basis of ROE data.[24] On the other hand, no experimental evidence for significant tail-to-tail (*t*-*t*) or "micelle" aggregations can be found. The same type of local structuration has been found for 1-butyl-3-methylimidazolium Tf_2N and 1-

butyl-2,3-dimethylimidazolium ILs. The comparison of the results of Table 1 with those of Tables 2 and 3 suggests that the contribution of the *h-h* motif decreases on going from pyrazolium **1** to dimethylpyrazolium **3** and **4**.

Further information on the aggregation motives and cation-anion interactions in the pure liquids can be obtained by heteronuclear (^{1}H-^{19}F)-NOE experiments (HOESY) of samples **1** and **3**, where the cations contain H atoms whilst the anions contain F atoms. The (^{1}H-^{19}F)-HOESY experiments on **1** and **3**, presented below in Figures 3 and 4, show different interactions between the fluorinated anion and the cations.

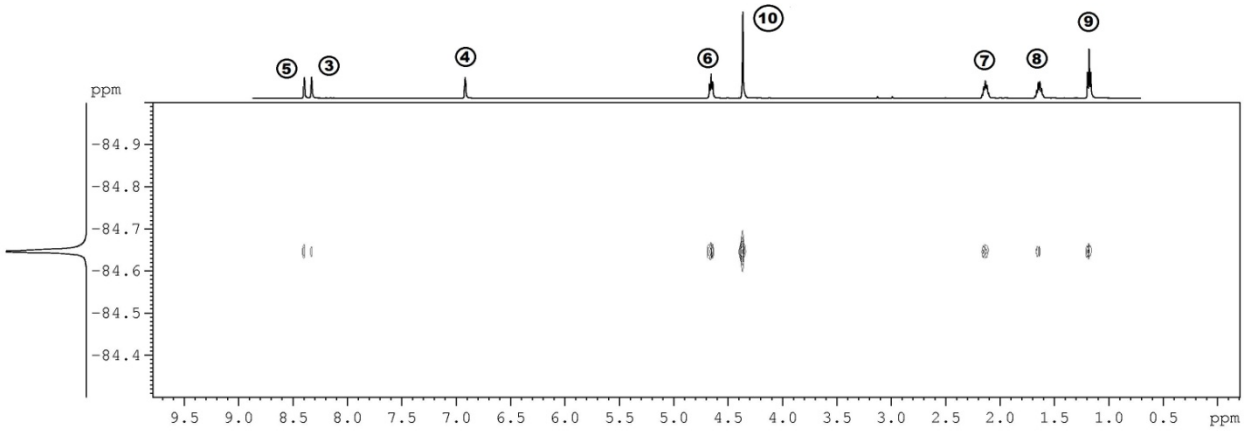

Figure 3. (^{1}H-^{19}F)-HOESY spectra of **1**. Top trace: ^{1}H-NMR spectrum with atom numbering for assignment. Vertical trace: ^{19}F-NMR spectrum.

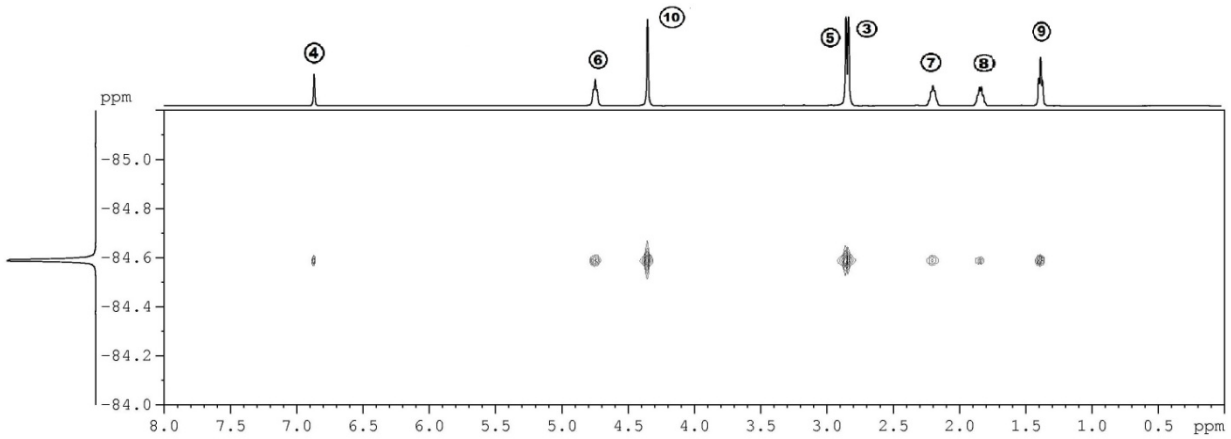

Figure 4. (^{1}H-^{19}F)-HOESY spectra of **3**. Top trace: ^{1}H-NMR spectrum with atom numbering for assignment. Vertical trace: ^{19}F-NMR spectrum.

The small but appreciable selectivity observed in HOESY of **1** suggests a correlated orientation of the anion and cation. The Tf_2N anion is close in space to the C(5)-N-N-C(3) frame (intermolecular distance of dipole-coupled nuclei < 4 Å, see Figure 1 for atom numbering) but does not show any appreciable interaction with H-C(4). This finding suggests a strikingly different behavior of pyrazole-based ILs compared to the homologous imidazolium derivatives, in which the H atom between the nitrogens displays some unique properties and specific interactions (acidity, H-bond donation, etc.). However, the NOEs of CF_3 groups with H atoms bonded to C(7), C(8) and C(9) of the butyl chain indicate a significant interaction of the anion with the apolar tail of the cation, which was not observed either in the case of [bmim][BF_4][28] or in the case of N-butyl-N-methyl pyrrolidinium Tf_2N^-.[29]

The HOESY spectrum of **3** indicates that the anion interacts in a non-selective way with the cation, thus suggesting an even minor degree of structuration with respect to **1**, probably due to the increased steric hindrance brought about by the methyl substitution.

3.3 Diffusion Coefficients, Density, Viscosity and Conductivity. Self-diffusion coefficients (*D*), density (ρ), viscosity (η) and conductivity (σ) were measured for all pyrazolium based ILs

after accurate drying, typically in the ranges T=293-353 K (for σ and η) and T=300-340 K (for D). Values measured at room temperature are given in Table 4, together with those reported for 1-ethyl-2-methylpyrazolium dicyanamides ([empz][$N(CN)_2$]) and three analogous imidazolium salts:[8] 1-ethyl-3-methylimidazolium dicyanamides ([emim][$N(CN)_2$]), 1-butyl-3-methylimidazolium dicyanamide ([bmim][$N(CN)_2$]) and 1-butyl-3-methylimidazolium bis(trifluoromethanesulfonyl)imide ([bmim][Tf_2N]). Table 4 contains also the Kamlet-Taft parameters π* (polarizability), α (hydrogen bond donor ability) and β (hydrogen bond acceptor ability), determined using three solvatochromic probes.

Table 4. Physico-chemical properties of pyrazolium- and imidazolium-based ILs at T=298 K.

Ionic Liquid	ρ (g/mL)	σ (mS/cm)	η (cP)	D_{cation}[b] (m^2/s)	D_{anion}[b] (m^2/s)	α	β	π*
[empz][$N(CN)_2$][a]	1.16[c]	17	24.6			0.428	Nd	1.11
[bmpz][Tf_2N]	1.40	3.20	67.1	$3.2*10^{-11}$	$2.6*10^{-11}$	0.69	0.205	1.04
[bmpz][$N(CN)_2$]	1.07	8.50	30.2			0.46	0.554	1.13
[bm_3pz][Tf_2N]	1.38	2.60	76.9	$2.4*10^{-11}$	$2.0*10^{-11}$	d	0.234	1.02
[bm_3pz][$N(CN)_2$]	1.05	3.20	77.0	$1.9*10^{-11}$		0.13	0.586	1.13
[bmim][Tf_2N]	1.43	4.60	40.0	$4.5*10^{-11}$	$3.6*10^{-11}$	0.64	0.248	0.97
[emim][$N(CN)_2$][a]	1.08[c]	28.0	16.1			0.53	nd	1.07
[bmim][$N(CN)_2$][a]	1.06[c]	11.0	29.3			0.46	0.708	1.12

[a] From ref 8. [b]The D values are measured at T=305 K. [c] From ref 8. Determined at 293 K. [d]Not determined due to the immediate disappearing of the colour after addition of the Reichardt's dye.

The self-diffusion coefficients D of the cations and the fluorine-containing anions were measured independently by PFGSE-NMR experiments in the ^{19}F and ^{1}H frequency domains,

respectively. The observed echo intensity I is related to the experimental parameters by the Stejskal-Tanner equation:[30]

$$I = I_0 \exp\left[-(\gamma g \delta)^2 D\left(\Delta - \frac{\delta}{3}\right)\right] \quad (3)$$

where I_0 is the echo intensity without field gradient, γ is the gyromagnetic ratio of the observed nucleus, g is the magnetic field gradient strength, δ is the duration of the field gradient and Δ is the interval between the two gradient pulses.

The measured diffusion coefficient of the cation and anion (for ILs **1** and **3**) follow the general trend $D_{\text{cation}} > D_{\text{anion}}$. This relationship points out that the cations' hydrodynamic radius is smaller than that of the anions, as previously reported for other classes of ILs.[29,31] The presence of two methyl groups in the cation (for ILs **3** and **4**) leads to a reduction of the diffusion coefficient. Similarly, the presence of the dicyanamide counterion slows down the diffusion of the bm_3pz cation, in comparison with Tf_2N.

All ILs display an approximate Arrhenius-type dependence of the diffusion coefficients on temperature:

$$D = D_0 e^{-E_D / RT} \quad (4)$$

where E_D is and activation energy for diffusion and R is the gas constant. The results are given in Table 5.

Table 5. Results of the Arrhenius fits of the ion diffusion coefficients.

Ionic liquid	$E_{D(\text{cation})}$ (kJ mol^{-1})	D_0 (m^{2}s^{-1})	R^2	$E_{D(\text{anion})}$ (kJ mol^{-1})	D_0	R^2
[bmpz][Tf_2N]	32.4	1.2*10^{-5}	0.997	33.1	1.3*10^{-5}	0.997

$[bm_3pz][Tf_2N]$	35.5	$3.0*10^{-5}$	0.993	38.8	$9.1*10^{-5}$	0.996
$[bm_3pz][N(CN)_2]$	41.7	$2.7*10^{-4}$	0.997			

For the present salts, in analogy with imidazolium based ILs, density and viscosity increase changing the anion from $[N(CN)_2]^-$ to $[Tf_2N]^-$ and their temperature dependencies approximately follow the Arrhenius equation (5) over the examined temperature range (20-80 °C),

$$\eta = \eta_0 e^{E_\eta / RT} \tag{5}$$

where E_η is the activation energy for viscous flow. However, the Arrhenius plots ($\ln\eta$ *vs.* $1/T$) of all investigated ILs show a slight upward curvature. Better fits of the viscosities were obtained using the Vogel-Fulcher-Tammann (VFT) law :

$$\eta = Ae^{B/(T-T_0)} \tag{6}$$

where A, B and T_0 are fitting parameters. Unlike the Arrhenius law, this allows a divergence of the viscosity at a finite T, consistently with a possible transition of these systems to supercooled and then to a glassy state (the fitted T_0 cannot be identified with a true glass transition temperature, though). The best parameters and correlation coefficients are reported in Table 6, together with the Arrhenius parameters. As generally found with other ILs, the VFT equation is able to predict more rigorously the viscosity behavior with temperature but, due to the limited accessible range of temperatures, does not allow to obtain clear-cut trends for the VFT parameters.

Table 6. Results of the Arrhenius and VFT fits of the viscosities.

Ionic liquid	E_η	η_0	R^2	A	B	T_0	R^2

	(kJ mol^{-1})	(cP)		(cP)	(K)	(K)	
[bmpz][Tf_2N]	28.3	$6.7\cdot10^{-4}$	0.990	0.91	356	215	0.998
[bm_3pz][Tf_2N]	29.9	$3.7\cdot10^{-4}$	0.992	0.40	523	198	0.999
[bmpz][$N(CN)_2$]	24.6	$1.5\cdot10^{-3}$	0.994	0.29	513	186	0.999
[bm_3pz][$N(CN)_2$]	32.3	$1.3\cdot10^{-4}$	0.990	0.76	224	224	0.997

The anion nature exerts a drastic effect on conductivity, as observed for viscosity. The conductivity of the present pyrazolium salts increases going from ILs having as counteranion $[Tf_2N]^-$ to $[N(CN)_2]^-$. As expected on the basis of the temperature dependence of the viscosities, also the conductivities follow approximately the Arrhenius equation (7):

$$\sigma = \sigma_0 e^{-E_\sigma / RT} \tag{7}$$

where E_σ is the activation energy for conductivity. Also these data have been fitted using the VFT equation:

$$\sigma = A e^{-B/R(T-T_0)} . \tag{8}$$

The best parameters and associated correlation coefficients are reported in Table 6, together with the Arrhenius parameters. Notice the fairly good agreement between the T_0's extracted from viscosity and conductivity measurements.

Table 7. Results of the Arrhenius and VFT fits of the conductivities.

Ionic liquid	E_σ kJ mol^{-1}	σ_0 mS cm^{-1}	R^2	A mS cm^{-1}	B K	T_0 K	R^2
[bmpz][Tf_2N]	13.0	$0.66\cdot10^{3}$	0.990	29.4	209	202	0.998
[bm_3pz][Tf_2N]	15.0	$1.2\cdot10^{3}$	0.992	39.5	282	193	0.999

[bmpz][$N(CN)_2$]	12.1	$1.1 \cdot 10^3$	0.996	96.0	298	174	0.999
[bm_3pz][$N(CN)_2$]	20.8	$15 \cdot 10^3$	0.986	79.0	271	213	0.997

Viscosity and diffusion are different manifestations of the fluid dynamics probed at molecular and atomistic level respectively. For pure ionic liquids[29] the activation energies needed for these processes is quite similar, while IL mixtures[32] revealed different values due presumably to nano-scale heterogeneity of these mixtures. For the two IL compounds [bmpz][Tf_2N] and [bm_3pz][Tf_2N], the values of the activation energies for the viscosity E_η are quite similar to those for the diffusive motion E_D. The variation of the cation structure does not produce a large change in these physico-chemical properties. On the other hand, [bm_3pz][$N(CN)_2$] has a value of E_D significantly higher than E_η. The comparison with [bm_3pz][Tf_2N] confirms that the dicyanamide anion increases the energy barrier for the diffusion. For all the studied compounds the conductivity process needs lower activation energies compared with viscosity and diffusion.

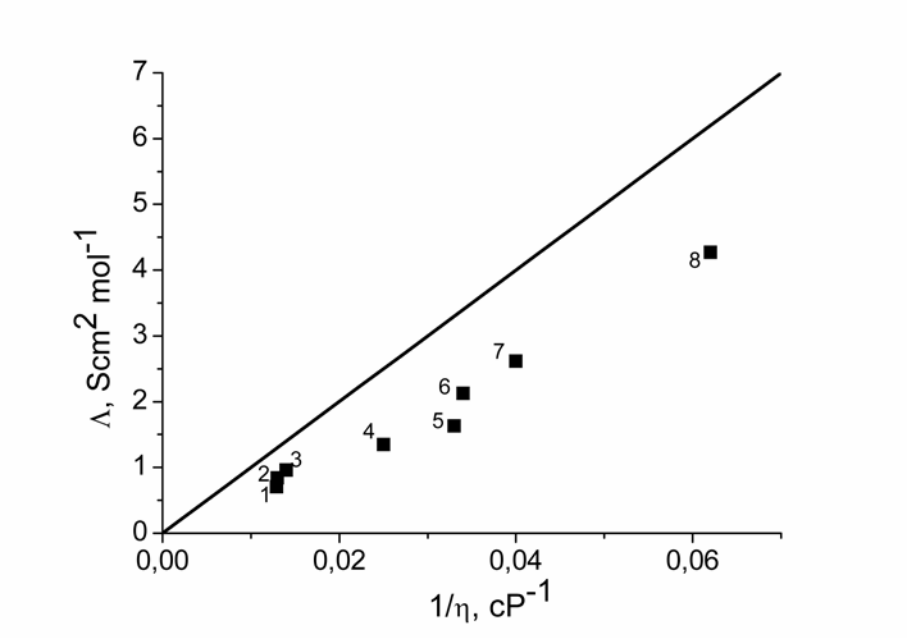

Figure 5. Walden plot at 25 °C: **1** [bm_3pz][$(CN)_2N$], **2** [bm_3pz][Tf_2N], **3** [bmpz][Tf_2N], **4** [bmim][Tf_2N], **5** [bmpz][$(CN)_2N$] and], **6** [bmim][$(CN)_2N$], **7** [empz][$(CN)_2N$], **8** [emim][$(CN)_2N$].

The comparison of the values of viscosity and conductivity for [bmpz][Tf_2N] and [bm_3pz][Tf_2N] shows that the introduction of two methyl groups on the cation core has only a moderate effect on both these properties, whereas a more significant effect is played by the same groups in the dicyanamide-based ILs. The low effect of the methyl groups in the case of bis(trifluoromethanesulfonyl)imides might have been anticipated, as it has been recently shown[7] that also the alkyl chain length in 1-alkyl-2,3,5-trimetheylpyrazolium bis(trifluoromethanesulfonyl)imides not significantly affect viscosity and conductivity. Considering that in the case of imidazolium salts the same structural features (alkyl chain length and presence of methyl group(s) on cation core) strongly affect both properties, the lower sensitivity of the pyrazolium cation-based ILs to ionic sizes might be attributed to the different anion-cation interaction ability and therefore to a different attitude of imidazolium and

pyrazolium cations to give organized three-dimensional structures (ion pairs and larger aggregates).

The unique properties of ILs arising from their nature of charged species able to aggregate are often expressed in terms of ionicity and defined on the basis of the Walden plot (Figure 5). According to the empirical Walden rule, the ionic mobility (represented by the equivalent conductivity Λ) is related to the fluidity ($1/\eta$) of the medium through which the ions move. The data for a 0.01 M aqueous KCl solution are taken as reference. All the data from Table 4 are plotted in Figure 5, which shows that the pyrazolium-based salts lie below the so-called Walden product line, roughly within the same region of the analogous imidazolium salts. The distance between the ideal line and the experimental data increase on going from $[Tf_2N]^-$ to $[N(CN)_2]^-$ based ILs and, in the case of $[Tf_2N]^-$, from pyrazolium to imidazolium. The departure of [bmpy][Tf_2N] and [bm_3py][Tf_2N] from the ideal Walden line is lower than that of [bmim][Tf_2N]. Since these deviations are generally considered indicative of the existence of a significant fraction of ion pairs and/or aggregation, the plot suggests a dependence of these phenomena on anion nature (both for pyrazolium and imidazolium based ILs aggregation increases on going from bis(trifluoromethylsulfonylimides) to dicyanamides) and cation nature (in the case of bis(trifluoromethylsulfonylimides)-based ILs, pyrazolium salts are nearest to the ideal line whereas a more complex behaviour characterizes dicyanamide-based salts).

Hydrodynamic theory relates the conductivity σ and diffusion through the approximate Nernst-Einstein equation:

$$\sigma_{NE} = \frac{nq^2}{kT}\left(D_+ + D_-\right) \tag{9}$$

where n is the number density of ions, $q=\pm e$ is the ion charge, k is Boltzmann's constant, T is the absolute temperature and D_+ and D_- are the cation and anion diffusion coefficients, respectively. The conductivities calculated from equation (9) are typically greater than the experimentally measured values (σ_{exp}) and this can be attributed to the neglect of ionic correlation effects. A graph of $\sigma_{exp}T$ *vs.* (D_++D_-) is reported in Figure 6 for compounds **1** and **3**. The plots demonstrate that $\sigma_{exp}<\sigma_{NE}$, as expected, but their values are still of the same order of magnitude, indicating a significant but not overwhelming degree of association.

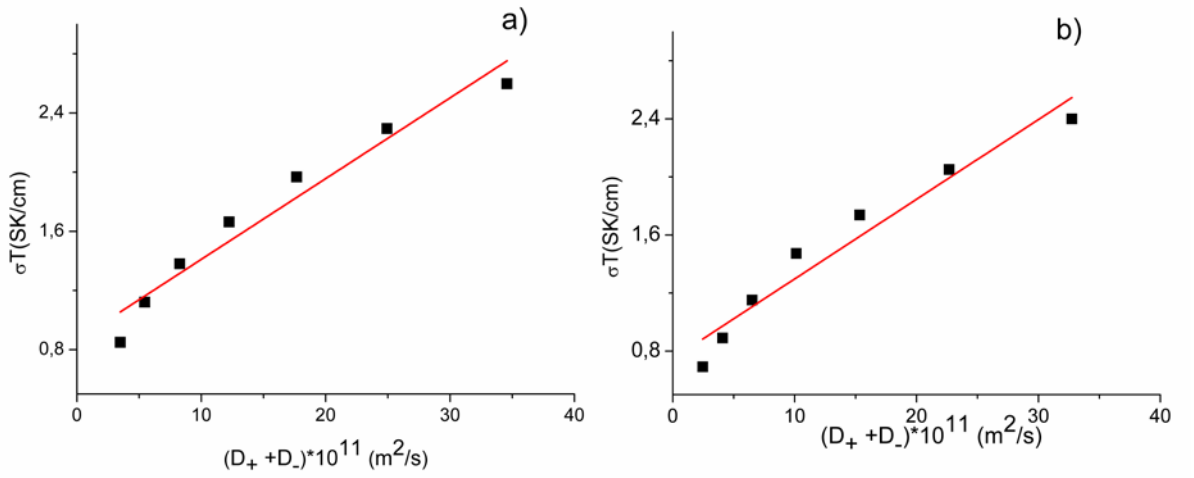

Figure 6. Graph of σT versus (D_++D_-) for [bmpz][Tf_2N] **a)** and [bm_3pz][Tf_2N] **b)**. The red lines are linear fits to the data.

The different propensity of the ILs depending on cation and anion structure to give ion association affects also the solvatochromic parameters.[33] As previously observed for imidazolium-based ionic liquids, the comparison of the Kamlet-Taft parameters found for the bis(trifluoromethanesulfonyl)imide and dicyanamide-based pyrazolium salts shows that [$N(CN)_2$]-based ILs are characterized by a slightly higher dipolarity/polarizability (π*), by a significantly higher hydrogen bond basicity (β), a parameter which is determined by the anion nature, and by a lower hydrogen bond acidity (α). The latter property, which is primarily

determined by the cation nature, is normally modulated by the anion basicity: a strong interaction between anion and cation, in other words ion association, reduces the cation's propensity to interact with Reichardt's dye. The solvatochromic parameters of pyrazolium and imidazolium salts show similar variations on going from (trifluoromethanesulfonyl)imides to dicyanamides suggesting an increased ion association in both systems. In addition, the 1,2-dialkylpyrazolium-based ILs have a hydrogen bond donor ability comparable to the 1,3-dialkylimidazolium salts. The α values characterizing [empz][$N(CN)_2$], [bmpz][$N(CN)_2$] and [bmpz][Tf_2N] are similar to those reported for analogous imidazolium salts, despite of the absence of the acidic proton at C(2). In pyrazolium salts the solvent-solute interaction with the dyes probably involves the other protons close to the nitrogen atoms. Only the introduction of two other methyl groups at C(3) and C(5) on the pyrazolium ring determines indeed a drastic reduction of the hydrogen bond donor ability. The interaction of the dye, as well as of the counteranion, with the protons H(3) and H(5) is eliminated and the interaction with H(7), H(8) and H(9) is reduced, probably by steric effects.

Conclusions

We have presented the synthesis and physico-chemical characterization of a new series of pyrazolium-based ILs. An environmental friendly procedure, based on the use of methylcarbonate as methylating agent, has been utilize for the first time to synthesize methylpyrazolium based ILs. NMR NOE experiments show specific head-to-tail and head-to-head aggregation motives, which are quite sensitive to steric effects produced by alkyl substitution of the cation. The nature of the anion also seems to influence the degree of nanostructuration. The heteronuclear HOESY experiments indicate the formation of loose ion pairs, easily disrupted by steric effects, thus confirming the tunability of the ion ordering in these systems.

Walden plot and Kamlet-Taft solvatochromic parameters suggest an increased ion association on going from bis(trifluoromethanesulfonyl)imide to dicyanamide-based pyrazolium salts. Furthermore, solvatochromic measurements show that 1,2-dialkylpyrazolium-based ILs have a hydrogen bond donor ability comparable to the 1,3-dialkylimidazolium salts, probably involving protons at C(3) and C(5) close to the nitrogen atoms. Only the introduction of two other methyl groups at these positions on the pyrazolium ring determines indeed a drastic reduction of the hydrogen bond donor ability.

The ion diffusion measured by NMR methods is significantly influenced not only by the cation size and steric hindrance ($D_{\text{cation}\mathbf{1}} > D_{\text{cation}\mathbf{3}}$), but also by the shape and size of the anion ($D_{\text{cation}\mathbf{3}} > D_{\text{cation}\mathbf{4}}$). The temperature dependencies of the viscosities, conductivities and diffusion show a similar Arrhenius-type behaviour characterized by close values of the activation energies for shear flow and diffusion processes. The VFT equation has also been used to fit the experimental parameters.

Chemical modulation of the steric hindrance of cation and the choice of the counter-ion open the possibility of an easy and extensive tunability of pyrazole-based ILs, as demonstrated by the Walden plot analysis, in order to design and tailor their physico-chemical properties for specific applications.

Supporting Information

NMR spectra of titled compounds, dihedral angles, interatomic distances, conformational energies of pyrazolium cations calculated at DFT level. This material is available free of charge via the Internet at http://pubs.acs.org.

Acknowledgments. The authors acknowledge the support of Regione Lombardia and CILEA Consortium through a LISA Initiative (Laboratory for Interdisciplinary Advanced Simulation)

2011 grant (http://lisa.cilea.it). FC, GR, AF and AM wish to thank the EU for funding (FP7 – GREENLION Project – Contract nº 285268).

References

(1) Plechkova, N. V.; Seddon, K. R. *Chem. Soc. Rev*. **2008**, *37*, 123–150.

(2) (a) Wasserscheid, P. and Welton, T. *Ionic liquids in Synthesis*, 2nd ED. Wiley–VCH, Weinheim**, 2008**. (b) Chiappe, C.; Pieraccini, D. *J.Phys. Org. Chem*. **2005**, *18*, 275–297.

(3) (a)Xiao, D.; Rajian, J. R.; Li, S.; Bartsch, R. A.; Quitevis, E. L. *J. Phys. Chem. B* **2006,** *110*, 16174–16178. (b) Xiao, D.; Rajian, J. R.; Cady A.; Li, S.; Bartsch, R. A.; Quitevis, E. L. *J. Phys. Chem. B* **2007,** *111*, 4669–4677. (c) Chiappe, C. *Monat fuer Chemie* **2007,** *138*, 1035–1043. (d) Bini, R.; Bortolini, O.; Chiappe, C.; Pieraccini, D.; Siciliano, T. *J. Phys. Chem. B* **2007,** *111*, 598–604.

(4) (a) Canongia Lopes, J. N.; Padua, A. A. H. *J. Phys. Chem. B* **2006,** *110*, 3330–3335. (b) Triolo, A.; Russina, O.; Bleif, H. J.; Di Cola, E. *J. Phys. Chem. B* **2007,** *111*, 4641–4644. (c) Gutel, T.; Santini, C. C.; Philippot, K.; Padua, A. A. H.; Pelzer, K.; Chaudert, B.; Chauvin, Y.; Basset, J. M. *J. Mater. Chem.* **2009,** *19*, 3624–3631. (d) Pensado, A. S.; Padua, A. A. H. *Angew. Chem. Int. Ed*. **2011,** *50*, 8683–8687.

(5) Umebayashi, Y.; Fukuda, S.; Kameda Y.; Kohara, S. *Research Frontiers*, **2007**, 118–119.

(6) (a) Abu_lebdeh, Y.; Abouimrane, A.; Alarco, P.–J.; Armand M. *J. Power Sources* **2006,** *154*, 255–261. (b) Seki, S.; Kabayashi, T.; Kabayashi, Y.; Takei, K.; Miyashiro, H.; Hayamizu, K.; Tsuzuki, S.; Mitsugi, T.; Umebayashi Y. *J. Mol. Liq.* **2010,** *152*, 9–13. (c) Ishimaru, N.;

Kubo, W.; Kitamura, T.; Yanagida, S.; Tsukahara, Y.; Maitani, M. M.; Wada Y. *Mat. Science & Eng B* **2011,** *176*, 996–1001.

(7) Yoshida, Y.; Baba, O.; Saito, G. *J. Phys. Chem. B* **2007**, *111*, 4742–4749.

(8) Seki, S.; Kabayashi, T.; Serizawa, N.; Kobayashi, Y.; Takei, K.; Miyashiro, H.; Hayamizu, K.; Tsuzuki, S.; Mitsugi, T.; Umebayashi, Y.; Watanabe M. *J. Power Sources* **2010,** *195*, 6207–6211.

(9) Desvaux, H.; Berthault, P.; Birlirakis, N.; Goldman, M.; Piotto, M. *J. Magn. Reson. Ser. A* **1995,** *113*, 47–52.

(10) (a) Alam, T. M.; Pedrotty, D. M.; Boyle, T. J. *Magn. Reson. Chem*. **2002,** *40*, 361–365. (b) Mantz, R. A.; Trulove, P. C.; Carlin, R. T.; Osteryoung, R. A. *Inorg. Chem*. **1995,** *34*, 3846–3847.

(11) Jerschow, A.; Mueller, N. *J. Magn. Reson. A* **1997,** *125*, 372–375.

(12) (a) Schmidt, M. W., Baldridge, K. K.; Boatz J. A.; Elbert, J, S. T.; Gordon, M. S.; Jensen, J. H.; Koseki, S.; Matsunaga, N.; Nguyen, K. A.; Su, S.; Windus, T. L.; Dupuis, M.; Montgomery, J. A. *J. Comput. Chem*. **1993,** *14*, 1347–1363. (b) Gordon, M. S.; Schmidt M. W. "Theory and Applications of Computational Chemistry, the first forty years" C. E. Dykstra, G. Frenking, K. S. Kim, G. E. Scuseria (editors), Elsevier, Amsterdam **2005,** 1167–1189.

(13) (a) Parr, R. G.; Yang, W. *"Density Functional Theory of Atoms and Molecules"*, Oxford Scientific, **1989**. (b) Koch, W.; Holthausen, M. C. *"A Chemist's Guide to Density Functional Theory"*, Wiley VCH **2001**. (c) Jensen, F. *"Introduction to Computational Chemistry"*, Wiley and Sons, Chichester **2007**.

(14) (a) Becke, A. D.; *J. Chem. Phys*. **1993**, *98*, 5648. (b) Stephens, P. J.; Devlin, F. J.; Chablowski, C. F.; Frisch, M. J. *J. Phys. Chem.* **1994**, *98*, 11623–11627. (c) Hertwig, R. H.; Koch, W. *Chem. Phys. Lett.* **1997,** *268*, 345–351.

(15) Krishnan, R.; Binkley, J. S.; Seeger, R.; Pople, J. A. *J. Chem. Phys*. **1980**, *72*, 650.

(16) Neuhaus D., Williamson M. P. "*The Nuclear Overhauser Effect in Structural and Conformational Analysis"*, second edition, Wiley–VCH, Inc., U.S.A. **2000**.

(17) Moreno, M.; Castiglione, F.; Mele, A.; Pasqui, C.; Raos G. *J. Phys. Chem. B* **2008**, *112*, 7826–7836.

(18) Holbrey, J. D.; Reichert, W. M.; Nieuwenhuyzen, M.; Johnston, S.; Seddon, K. R.; Rogers, R. D. *Chem. Commun*. **2003**, 1636–1637.

(19) Saha, S.; Hayashi, S.; Kobayashi, A.; Hamaguci, H. *Chem. Lett.* **2003**, *32*, 740–741.

(20) Golovanov, G.; Lyssenko, K. A.; Antipin, M. Y.; Vygodskii, Y. S.; Lozinskaya, E. I.; Shaplow, A. S. *Cryst. Growth Design* **2005,** *5*, 337–340.

(21) Choudhury, A. R.; Winterton, N.; Steiner, A.; Cooper, A. I.; Johnson, K. A. *J. Am. Chem. Soc*. **2005,** *127*, 16792–16793.

(22) (a) Kölle, P.; Dronskowski, R. *Eur. J. Inorg. Chem*. **2004,** 2313–2320. (b) Kölle, P.; Dronskowski, R. *Inorg. Chem*. **2004,** *43*, 2803–2809.

(23) Mele, A.; Tran, C. D.; De Paoli Lacerda S. H. *Angew. Chem. Int. Ed*. **2003**, *42*, 4264–4266.

(24) (a) Mele A.; , Romanò, G.; Giannone, M.; Ragg, E.; Fronza, G.; Raos, G.; Marcon, V. *Angew. Chem. Int. Ed. Engl*. **2006**, *45*, 1123–1126. (b) Mele A. *Chimica Oggi / Chemistry Today*, **2010**, *28*, 48–55.

(25) Gutel, T.; Santini, C. C.; Pàdua, A. A. H.; Fenet, B.; Chauvin, Y.; Canongia Lopes, J. N.; Bayard, F.; Costa Gomes, M. F.; Pensado, Alfonso S. *J. Phys. Chem. B* **2009,** *113*, 170–177.

(26) Phung Le, M. L.; Alloin, F.; Strobel, P.; Leprêtre, J.–C.; Perez del Valle, C.; Judeinstein, P. *J. Phys. Chem. B* **2010,** *114*, 894–903.

(27) Puttick, S.; Davis, A. L.; Butler, K.; Lambert, L.; El harfi, J.; Irvine, D. J.; Whittaker, A. K.; Thurecht, K. J.; Licence, P. *Chem. Sci*. **2011**, *2*, 1810–1816.

(28) Mele A. "Investigation of the Structure of 1-Butyl-3-methylimidazolium Tetrafluoroborate and Its Interaction with Water by Homo- and Heteronuclear Overhauser Enhancement in Ionic Liquids III: Fundamentals, Progress, Challenges, and Opportunities", R.D. Rogers and K. Seddon, Eds. ACS Symposium Serie 901, American Chemical Society: Washington DC, **2005**, pp. 2-17.

(29) Castiglione, F.; Moreno, M.; Raos, G.; Famulari, A.; Mele, A.; Appetecchi, G. B.; Passerini S. *J. Phys. Chem. B* **2009,** *113*, 10750–10759.

(30) Stejskal, O.E.; Tanner, J.E. *J. Chem. Phys.* **1965,** *42*, 288.

(31) Noda, A.; Hayamizu, K.; Watanabe, M. *J. Phys. Chem. B* **2001,** *105*, 4603–4610.

(32) Castiglione, F.; Raos, G.; Appetecchi, G. B.; Montanino, M.; Passerini S.; Moreno, M.; Famulari A.; Mele, A. *Phys. Chem. Chem. Phys.* **2010,** *12*, 1784–1792.

(33) Chiappe C.; Pomelli, C. S; Rajamani S. *J. Phys. Chem. B* **2011**, *115*¸9653–9661.